Yukawa coupling unification in an $\mathrm{SO}(10)$ model consistent with Fermilab $(g-2)_\mu$ result

Amin Aboubrahim,[a] Pran Nath[b] and Raza M. Syed[c]

[a] *Institut für Theoretische Physik, Westfälische Wilhelms-Universität Münster,*
Wilhelm-Klemm-Straße 9, 48149 Münster, Germany

[b] *Department of Physics, Northeastern University,*
Boston, MA 02115-5000, U.S.A.

[c] *Department of Physics, American University of Sharjah,*
P.O. Box 26666, Sharjah, U.A.E.[1]

E-mail: aabouibr@uni-muenster.de, p.nath@northeastern.edu, rsyed@aus.edu

ABSTRACT: We investigate the Yukawa coupling unification for the third generation in a class of SO(10) unified models which are consistent with the $4.2\,\sigma$ deviation from the standard model of the muon $g-2$ seen by the Fermilab experiment E989. A recent analysis in supergravity grand unified models shows that such an effect can arise from supersymmetric loops correction. Using a neural network, we further analyze regions of the parameter space where Yukawa coupling unification consistent with the Fermilab result can appear. In the analysis we take into account the contributions to Yukawas from the cubic and the quartic interactions. We test the model at the high luminosity and high energy LHC and estimate the integrated luminosities needed to discover sparticles predicted by the model.

---

[1]Permanent address.

Contents

1 Introduction

Recently the Fermilab E989 experiment [1] has measured $a_\mu = (g-2)_\mu/2$ with significantly greater accuracy than the previous Brookhaven experiment [2, 3]. Thus the combined Fermilab experimental data and Brookhaven experimental data gives

$$a_\mu^{\mathrm{exp}} = 116592061(41) \times 10^{-11} \, , \tag{1.1}$$

which is to be compared with the Standard Model (SM) prediction [4]

$$a_\mu^{\mathrm{SM}} = 116591810(43) \times 10^{-11}. \tag{1.2}$$

The combined Fermilab and Brookhaven result shows an excess over the SM result by an amount $\Delta a_\mu^{\mathrm{FB}}$ which is

$$\Delta a_\mu^{\mathrm{FB}} = a_\mu^{\mathrm{exp}} - a_\mu^{\mathrm{SM}} = 251(59) \times 10^{-11}. \tag{1.3}$$

Eq. (1.3) records a 4.2σ deviation from the SM compared to 3.7σ for the Brookhaven result. hus the Fermilab experiment further strengthens the Brookhaven result on the possible existence of new physics beyond the Standard Model (see, however, ref. [5]). Subsequent to the Fermilab result, artificial neural network analysis was used to explore the parameter space of supergravity (SUGRA) unified models. It was seen that regions of the parameter space where supersymmetric loops can give the desired correction consistent with the Fermilab results are those where gluino-driven radiative breaking of the electroweak symmetry

occurs [6], a region referred to as $\tilde{g}$SUGRA [7–9]. Using a neutral network we investigate this region further to explore the region where Yukawa unification in an SO(10) model [9] can occur consistent with the Fermilab result.

The outline of rest of the paper is as follows: in section 2 details of the SO(10) model are discussed. In section 3 an analysis of the parameter space of SUGRA SO(10) model which gives Yukawa coupling unification consistent with the Fermilab $g - 2$ result is given. Here the light and the heavy sparticle spectrum is also computed. In section 4, simulations for the observation of the sparticles predicted by the model at HL-LHC and HE-LHC are given. Conclusions are given in section 5. Some further details of the model are given in the appendix.

2 The model

The general class of SO(10) models we consider are those of [10, 11] with [9] being one of them which are similar in spirit to the missing partner SU(5) models [12, 13]. These models involve large Higgs representations such as $126 + \overline{126}$, 210, 120 for Yukawa couplings. Large Higgs representations have been used in several early works [14–16] and also more recently, e.g., [17–23] and the references therein (for a review of SO(10) models, see ref. [24]). In the model we consider [9, 11], the missing partner mechanism comes about as follows: the Higgs sector consists of the fields $126 + \overline{126}$, 210, $2 \times 10 + 120$ set of representations. The fields $126 + \overline{126}$, 210 are heavy which break the GUT symmetry down to the SM gauge group symmetry, while the $2 \times 10 + 120$ Higgs fields are light. The heavy fields contain 3 pairs of heavy Higgs doublets while the light fields have four pairs of light Higgs doublets. When the light and heavy fields mix, three pairs of the light Higgs doublets become heavy while one combination of the light doublets remains light and is identified as the Higgs field of the MSSM. We give below further details of the model used in this analysis.

The superpotential of the SO(10) model is given by [9]

$$W = W_{\text{GUT}} + W_{\text{DT}} + W_{\text{Yuk}}, \tag{2.1}$$

where

$$
\begin{aligned}
W_{\text{GUT}} &= M^{126}\Delta_{\mu\nu\rho\sigma\lambda}\overline{\Delta}_{\mu\nu\rho\sigma\lambda} + M^{210}\Phi_{\mu\nu\rho\sigma}\Phi_{\mu\nu\rho\sigma} + \eta\Phi_{\mu\nu\rho\sigma}\Delta_{\mu\nu\lambda\tau\xi}\overline{\Delta}_{\rho\sigma\lambda\tau\xi} \\
&\quad + \lambda\Phi_{\mu\nu\rho\sigma}\Phi_{\rho\sigma\lambda\tau}\Phi_{\lambda\tau\mu\nu}\,,
\end{aligned} \tag{2.2}
$$

$$
\begin{aligned}
W_{\text{DT}} &= a\,{}^{1}\Omega_{\mu}\overline{\Delta}_{\mu\nu\rho\sigma\lambda}\Phi_{\nu\rho\sigma\lambda} + \sum_{r=1}^{2} b_r\,{}^{r}\Omega_{\mu}\Delta_{\mu\nu\rho\sigma\lambda}\Phi_{\nu\rho\sigma\lambda} + c\,\Sigma_{\mu\nu\rho}\Delta_{\nu\rho\sigma\lambda\tau}\Phi_{\mu\sigma\lambda\tau} \\
&\quad + \overline{c}\,\Sigma_{\mu\nu\rho}\overline{\Delta}_{\nu\rho\sigma\lambda\tau}\Phi_{\mu\sigma\lambda\tau}\,.
\end{aligned} \tag{2.3}
$$

The notation used above is as follows: $\Delta_{\mu\nu\rho\sigma\lambda}$ and $\overline{\Delta}_{\mu\nu\rho\sigma\lambda}$ are fields for the 126 and $\overline{126}$ representations, $\Phi_{\mu\nu\rho\sigma}$ is the field for the 210 representation and ${}^{r}\Omega_{\mu}(r = 1, 2)$ are the fields for the two 10 of Higgs representations and $\Sigma_{\mu\nu\rho}$ is the field for the 120-plet representation. In the above W_{GUT} breaks the SO(10) GUT symmetry down to the standard model gauge group $\text{SU}(3)_C \times \text{SU}(2)_L \times \text{U}(1)_Y$ by VEV formations of $\mathcal{V}_{1_{126}}$ and $\mathcal{V}_{1_{\overline{126}}}$ and the VEVs of

$\mathcal{V}_{1_{210}}$, $\mathcal{V}_{24_{210}}$, $\mathcal{V}_{75_{210}}$. The equations that determine these VEVs are derived in [9]. Thus the $126 + \overline{126}$-plet VEVs $\mathcal{V}_{1_{126}}$ and $\mathcal{V}_{1_{\overline{126}}}$ break the SO(10) symmetry down to SU(5) × U(1) and the 210-plet VEVs $\mathcal{V}_{1_{210}}$, $\mathcal{V}_{24_{210}}$, $\mathcal{V}_{75_{210}}$ further break the gauge symmetry down to SU(3)$_C$ × SU(2)$_L$ × U(1)$_Y$. The notation for the VEVs is explicit. Thus, for example, $\mathcal{V}_{1_{126}}$ stands for the VEV of the SU(5) singlet in the SU(5) × U(1) decomposition of 126 and $\mathcal{V}_{24_{210}}$ stands for the VEV of the 24-plet of SU(5) field in the SU(5) × U(1) decomposition of 210. The doublet-triplet splitting is generated by W_{DT} which contains $2 \times 10 + 120$-plets of light fields. Thus the heavy fields $126 + \overline{126}$-plet and 210-plet contain three heavy SU(2) Higgs doublet pairs while the light fields $2 \times 10 + 120$-plets contain four light Higgs doublet pairs. After mixing of the light and heavy fields, three light Higgs doublets become heavy leaving one pair massless which we identify as the standard model Higgs doublet.

The Yukawa couplings arise from cubic and quartic interactions. They are given by

$$W_{\mathrm{Yuk}} = W_3 + W_4, \tag{2.4}$$

where

$$W_3 = \sum_{r=1}^{2} f^{10_r} \langle \Psi_{(+)}^* | B\Gamma_\mu | \Psi_{(+)} \rangle \, {}^r\Omega_\mu. \tag{2.5}$$

Here B and Γ's are the SO(10) charge conjugation and gamma matrices [17] and W_4 are the higher dimensional interactions discussed below. Yukawa couplings arising from eq. (2.5) are given by

$$\mathcal{L}_{\mathrm{Yuk}} = +h_\tau^0 \, \epsilon^{ab} \mathbf{H_d}_a \mathbf{L}_b \mathbf{E^c} - h_b^0 \, \mathbf{H_d}_a \mathbf{Q}^{a\alpha} \mathbf{D}_\alpha^\mathsf{c} - h_t^0 \, \epsilon_{ab} \mathbf{H_u}^a \mathbf{Q}^{b\alpha} \mathbf{U}_\alpha^\mathsf{c} + \text{h.c.}, \tag{2.6}$$

where

$$h_\tau^0 = i2\sqrt{2} \sum_{r=1}^{2} f^{10_r} V_{d_{r1}}, \quad h_b^0 = -i2\sqrt{2} \sum_{r=1}^{2} f^{10_r} V_{d_{r1}}, \quad h_t^0 = -i2\sqrt{2} \sum_{r=1}^{2} f^{10_r} U_{d_{r1}}, \tag{2.7}$$

where $U_{d_{r1}}$ and $V_{d_{r1}}$ are defined by eq. (2.14) and evaluated numerically in tables 2 and 3. In addition to Yukawa couplings arising from W_3, contributions arise from higher dimensional operators in W_4 where

$$W_4 = W_4^{(1)} + W_4^{(2)} + W_4^{(3)}, \tag{2.8}$$

and where

$$W_4^{(1)} = -\frac{f^{(1)}}{5!M_c} b_r \langle \Psi_{(+)}^* | B\Gamma_{[\lambda}\Gamma_\mu\Gamma_\nu\Gamma_\rho\Gamma_{\sigma]} | \Psi_{(+)} \rangle \, [{}^r\Omega_\lambda \Phi_{\mu\nu\rho\sigma} - {}^r\Omega_\mu \Phi_{\lambda\nu\rho\sigma} + {}^r\Omega_\nu \Phi_{\lambda\mu\rho\sigma}$$
$$- {}^r\Omega_\rho \Phi_{\lambda\mu\nu\sigma} + {}^r\Omega_\sigma \Phi_{\lambda\mu\nu\rho}], \tag{2.9}$$

$$W_4^{(2)} = -\frac{f^{(2)}}{5!M_c} \langle \Psi_{(+)}^* | B\Gamma_{[\lambda}\Gamma_\mu\Gamma_\nu\Gamma_\rho\Gamma_{\sigma]} | \Psi_{(+)} \rangle \, [\Sigma_{\lambda\alpha\beta} \Phi_{\gamma\rho\sigma\lambda} - \Sigma_{\lambda\alpha\gamma} \Phi_{\beta\rho\sigma\lambda} + \Sigma_{\lambda\alpha\rho} \Phi_{\beta\gamma\sigma\lambda}$$
$$- \Sigma_{\lambda\alpha\sigma} \Phi_{\beta\gamma\rho\lambda} - \Sigma_{\lambda\gamma\beta} \Phi_{\alpha\rho\sigma\lambda} + \Sigma_{\lambda\rho\beta} \Phi_{\alpha\gamma\sigma\lambda}$$
$$- \Sigma_{\lambda\sigma\beta} \Phi_{\alpha\gamma\rho\lambda} - \Sigma_{\lambda\gamma\rho} \Phi_{\beta\alpha\sigma\lambda} + \Sigma_{\lambda\gamma\sigma} \Phi_{\beta\alpha\rho\lambda}$$
$$- \Sigma_{\lambda\rho\sigma} \Phi_{\beta\alpha\gamma\lambda}], \tag{2.10}$$

$$W_4^{(3)} = \frac{f^{(3)}}{M_c} \langle \Psi_{(+)}^* | B\Gamma_\mu | \Psi_{(+)} \rangle \Sigma_{\rho\sigma\lambda} \Phi_{\rho\sigma\lambda\mu}. \tag{2.11}$$

Thus W_4 gives additional contributions to the Yukawa couplings for the third generation which we denote by δh_t, δh_b, δh_τ which are evaluated in the appendix. The total Yukawa couplings arising from eq. (2.4) is then given by

$$h_t = h_t^0 + \delta h_t, \quad h_b = h_b^0 + \delta h_b, \quad h_\tau = h_\tau^0 + \delta h_\tau, \tag{2.12}$$

where h_b, h_t, h_τ act as boundary conditions on Yukawas of b, t, τ which are evolved down to the electroweak scale Q where they are related to b, t, τ masses so that

$$m_t(Q) = \frac{h_t(Q)v\sin\beta}{\sqrt{2}}, \quad m_b(Q) = \frac{h_b(Q)v\cos\beta}{\sqrt{2}}, \quad m_\tau(Q) = \frac{h_\tau(Q)v\cos\beta}{\sqrt{2}}. \tag{2.13}$$

Here we used the relations $\langle H_d \rangle = \frac{v}{\sqrt{2}}\cos\beta$ and $\langle H_u \rangle = \frac{v}{\sqrt{2}}\sin\beta$, and where $v = 246\,\text{GeV}$.

As noted above there are seven Higgs doublet pairs three of which are heavy and four are light, and after the mixing of the light and heavy fields three pairs of light Higgs doublets become heavy and one pair remains light. To extract the light Higgs doublets we need to diagonalize the 7×7 Higgs doublet mass matrix given in [9]. The Higgs doublet mass matrix is not symmetric and is diagonalized by two unitary matrices U_d and V_d. Thus the down Higgs and the up Higgs doublet mass matrices are diagonalized by the transformation

$$\mathcal{H}_d = V_d \mathcal{H}'_d, \quad \mathcal{H}_u = U_d \mathcal{H}'_u, \tag{2.14}$$

where

$$\mathcal{H}_d^T = \left({}^{(\bar{5}10_1)}\mathsf{D}_a, {}^{(\bar{5}10_2)}\mathsf{D}_a, {}^{(\bar{5}120)}\mathsf{D}_a, {}^{(\bar{5}126)}\mathsf{D}_a, {}^{(\bar{5}210)}\mathsf{D}_a, {}^{(\overline{45}120)}\mathsf{D}_a, {}^{(\overline{45}\overline{126})}\mathsf{D}_a\right), \tag{2.15}$$

$$\mathcal{H}_d'^T = \left(\mathbf{H}_{\mathbf{d}a}, {}^2\mathsf{D}'_a, {}^3\mathsf{D}'_a, {}^4\mathsf{D}'_a, {}^5\mathsf{D}'_a, {}^6\mathsf{D}'_a, {}^7\mathsf{D}'_a\right), \tag{2.16}$$

$$\mathcal{H}_u^T = \left({}^{(\bar{5}10_1)}\mathsf{D}^a, {}^{(\bar{5}10_2)}\mathsf{D}^a, {}^{(\bar{5}120)}\mathsf{D}^a, {}^{(\bar{5}126)}\mathsf{D}^a, {}^{(\bar{5}210)}\mathsf{D}^a, {}^{(\overline{45}120)}\mathsf{D}^a, {}^{(\overline{45}\overline{126})}\mathsf{D}^a\right), \tag{2.17}$$

$$\mathcal{H}_u'^T = \left(\mathbf{H}_{\mathbf{u}}{}^a, {}^2\mathsf{D}^{a\prime}, {}^3\mathsf{D}^{a\prime}, {}^4\mathsf{D}^{a\prime}, {}^5\mathsf{D}^{a\prime}, {}^6\mathsf{D}^{a\prime}, {}^7\mathsf{D}^{a\prime}\right). \tag{2.18}$$

In the above the notation is as follows: ${}^{(\bar{5}10_1)}$ stands for the down Higgs doublet in the $\mathrm{SU}(5) - \bar{5}$-plet in the 10_1 which is one of the two 10-plets of light Higgs of $\mathrm{SO}(10)$. Further, D's and D''s represent the normalized kinetic energy basis and normalized kinetic and mass eigenbasis, respectively of the Higgs doublet mass matrix. The pair of doublets $(\mathbf{H}_{\mathbf{d}a}, \mathbf{H}_{\mathbf{u}}{}^a)$ are identified to be light and are the normalized electroweak Higgs doublets of the minimal supersymmetric standard model (MSSM). The matrix elements of U_d and V_d relevant in our analysis below are those elements that connect the light doublets, i.e., $U_{d_{11}}, U_{d_{21}}, \cdots . U_{d_{71}}$, and the elements $V_{d_{11}}, V_{d_{21}}, \cdots, V_{d_{71}}$. Other matrix elements of U_d and V_d do not contribute in the low energy theory. As noted above the explicit form of the 7×7 Higgs doublet mass matrix is given in [9]. The U and the V matrices are obtained by diagonalization of this matrix. Numerical values of the non-zero matrix elements of U_d and V_d relevant in the analysis are displayed in tables 2 and 3 for benchmarks of table 1.

3 SO(10) SUGRA model with Yukawa unification consistent with Fermilab $(g-2)_\mu$

Since the muon $g-2$ is one of the most accurately determined quantities in physics even a small deviation from the standard model prediction would be a significant indicator of new physics. For example, it is known that supersymmetric loop corrections could be of the same size as the electroweak corrections in the SM [25–30]. Indeed the Brookhaven result in 2001 [2] resulted in several works pointing out the impact on physics expected at colliders and elsewhere [31–40]. Thus the experiment became one of the important constraints on the parameter space of SUSY models. The discovery of the Higgs boson at 125 GeV further constrained the parameter space implying that the size of weak SUSY scale could be large lying in the TeV region [41–45]. Since the Fermilab result has indicated more strongly than the Brookhaven experiment for the existence of new physics, it is interesting to ask how the $b-t-\tau$ unification is affected [1]. The early work of [46] pointed out that such a unification could occur in SO(10) with appropriate choice of soft parameters. Such a unification has important effects on other phenomena such as dark matter (DM) [47]. Thus it is of interest to ask if $b-t-\tau$ unification can come about consistent with Fermilab data. We investigate this question using a neural network which is found to be useful in the analysis of large parameter spaces [48, 49]).

The analysis is done within the framework of supergravity grand unified models [50–52] using non-univeralities of gaugino masses [53–62]. The scan of the SUGRA parameter space is performed using an artificial neutral network (ANN) implemented in xBIT [63]. The ANN has three layers with 25 neurons per layer. It constructs the likelihood of a point using the three constraints on the Higgs mass, DM relic density and muon $g-2$, i.e.,

$$m_{h^0} = 125 \pm 2 \text{ GeV},$$
$$\Omega h^2 < 0.126,$$
$$\Delta a_\mu = (2.87 \pm 0.97) \times 10^{-9}.$$

The ANN first generates a set of points using the SUGRA input parameters which are used to train the neutral network based on the constructed likelihood function. The input parameters are m_0, A_0, m_1, m_2, m_3 and $\tan\beta$ where m_0 is the universal scalar mass, A_0 is the universal trilinear coupling, m_1, m_2, m_3 are the $U(1), SU(2), SU(3)$ gaugino masses all at the GUT scale and $\tan\beta = \langle H_u \rangle / \langle H_d \rangle$ where H_u gives mass to the up quarks and H_d gives mass to the down quarks and the charged leptons. We notice that the ANN predicts a particle spectrum consistent with $\tilde{g}$SUGRA where the colored sparticles are heavy and the sleptons, staus and electroweakinos are lighter. Generating the sparticle spectrum requires evolving the renormalization group equations (RGEs) and for this we use SPheno-4.0.4 [64, 65] which implements two-loop MSSM RGEs and three-loop SM RGEs while taking into account SUSY threshold effects at the one-loop level. The larger SUSY scale makes it necessary to employ a two-scale matching condition at the electroweak and SUSY scales [66] thereby improving the calculations of the Higgs boson mass and of the sparticle spectrum. The bottom quark mass and α_S (the fine structure constant for the

Model	η	λ	M^{126}	M^{210}	$\mathcal{V}_{1_{210}}$	$\mathcal{V}_{24_{210}}$	$\mathcal{V}_{75_{210}}$	$\mathcal{V}_{1_{126}}$
(a)	2.22	1.96	5.73×10^{17}	1.14×10^{15}	2.00×10^{18}	$(-4.00 + \imath 0.42) \times 10^{18}$	$(-8.97 + \imath 0.38) \times 10^{18}$	$(2.82 - \imath 0.09 i) \times 10^{17}$
(b)	2.85	2.31	8.10×10^{17}	2.00×10^{16}	2.20×10^{18}	-4.01×10^{18}	-2.08×10^{18}	$\imath 2.93 \times 10^{18}$
(c)	3.00	2.88	4.27×10^{17}	2.12×10^{15}	1.10×10^{18}	$(-2.19 + \imath 0.36) \times 10^{18}$	$(-4.94 + \imath 0.32) \times 10^{18}$	$(2.45 - \imath 0.12) \times 10^{17}$
(d)	2.62	0.63	4.31×10^{17}	4.01×10^{15}	1.28×10^{18}	-2.27×10^{18}	-1.15×10^{18}	$\imath 9.20 \times 10^{17}$
(e)	1.37	2.61	5.67×10^{17}	1.41×10^{16}	3.20×10^{18}	$(-6.32 + \imath 1.65) \times 10^{18}$	$(-1.45 + \imath 0.15) \times 10^{19}$	$(1.60 - \imath 0.12) \times 10^{18}$
(f)	1.11	2.51	3.03×10^{17}	1.44×10^{16}	2.12×10^{18}	$(-4.16 + \imath 1.39) \times 10^{18}$	$(-9.65 + \imath 1.27) \times 10^{18}$	$(1.46 - \imath 0.14) \times 10^{18}$
(g)	2.24	0.90	4.04×10^{17}	2.89×10^{15}	1.40×10^{18}	-2.65×10^{18}	-1.42×10^{18}	$\imath 1.33 \times 10^{18}$
(h)	2.98	2.71	5.09×10^{17}	1.79×10^{16}	1.32×10^{18}	$(-2.54 + \imath 1.19) \times 10^{18}$	$(-6.09 + \imath 1.11) \times 10^{18}$	$(7.83 - \imath 1.04) \times 10^{17}$
(i)	2.07	1.13	3.11×10^{17}	1.21×10^{16}	1.16×10^{18}	-1.86×10^{18}	-8.71×10^{17}	$\imath 1.21 \times 10^{18}$
(j)	2.99	0.39	6.61×10^{17}	1.88×10^{16}	1.71×10^{18}	-1.58×10^{18}	-4.80×10^{17}	$\imath 7.54 \times 10^{17}$

Table 1. A numerical estimate of the VEVs of the Standard Model singlets in 210, 126 and $\overline{126}$-plets arising in the spontaneous breaking of the SO(10) GUT gauge symmetry under the assumption $\mathcal{V}_{1_{126}} = \mathcal{V}_{1_{\overline{126}}}$. All VEVs and masses are in GeV.

$SU(3)_C)$ are run up to the scale of the Z boson mass, M_Z, using four-loop RGEs in the $\overline{\text{MS}}$ scheme while for the top quark, the evolution starts at the pole mass and the $\overline{\text{MS}}$ mass is computed by running down to the M_Z scale including two-loop QCD corrections. The tau mass is calculated at M_Z including one-loop electroweak corrections. The calculation of the $\overline{\text{MS}}$ Yukawas at the electroweak scale involves the first matching conditions to include SM thresholds. Those couplings are then run using 3-loop SM RGEs to M_{SUSY} where the second matching takes place to include SUSY thresholds at the one-loop level and a shift is made to the $\overline{\text{DR}}$ scheme. The 2-loop MSSM RGEs of the $\overline{\text{DR}}$ Yukawas and gauge couplings are then run to the GUT scale where the soft SUSY breaking boundary conditions are applied. The obtained set of points are then passed to `Lilith` [67, 68], `HiggsSignals` [69] and `HiggsBounds` [70] to check the Higgs sector constraints as well as `SModelS` [71–73] to check the LHC constraints. Furthermore, `microOMEGAs-5.2.7` [74] has a module which we use to check the constraints from DM direct detection experiments.

We discuss now the results of our analysis. In table 1 we give an analysis of the VEVs of the heavy fields that enter in the GUT symmetry breaking for a range of GUT parameters η, λ, M^{126} and M^{210} where the VEVs are in general complex. The VEVs are obtained by solving the spontaneous symmetry breaking equations using W_{GUT}. Using the VEVs of table 1, one solves for the Higgs doublet mass matrix using a range of $a, b_1, b_2, c, \bar{c}$ that appear in W_{DT}. The diagonalization of the Higgs mass matrix allows us to identify the linear combination of the Higgs doublet fields which are massless and correspond to the pair of MSSM Higgs.

The diagonalization also allows for computation of non-vanishing elements of the U and V matrices that connect to the light Higgs. These are the matrix elements $U_{d_{11}}$, $U_{d_{21}}$, $U_{d_{31}}$, $U_{d_{61}}$ and the matrix elements $V_{d_{11}}$, $V_{d_{21}}$, $V_{d_{31}}$, $V_{d_{61}}$. They are listed in tables 2 and 3. In table 4 we give a list of parameters that enter in the cubic couplings W_3 and in the quartic couplings W_4. In table 5 we give the computations of the contributions of the cubic couplings, the quartic couplings and their sum for b, t, τ for the model points of table 1. Computation of b, t, τ masses using the analysis of table 5 as boundary conditions at the GUT scale and using RG evolution down to the electroweak scale is given in table 6. An analysis of the Higgs boson mass, the light sparticle masses, the dark matter relic

Model	a	b_1	b_2	c	$\bar{c}$	$U_{d_{11}}$	$U_{d_{21}}$	$U_{d_{31}}$	$U_{d_{61}}$
(a)	0.22	1.86	1.14	1.46	0.18	$-0.034 + \imath 0.051$	$0.298 + \imath 0.285$	$0.231 + \imath 0.351$	$-0.495 - \imath 0.636$
(b)	2.03	2.50	2.70	0.81	1.15	$-0.040 - \imath 0.015$	$0.082 + \imath 0.030$	$0.185 + \imath 0.067$	$-0.917 - \imath 0.333$
(c)	1.70	2.95	1.21	0.21	2.74	$-0.163 - \imath 0.009$	$0.381 + \imath 0.080$	$-0.098 + \imath 0.409$	$0.091 - \imath 0.798$
(d)	0.27	2.55	2.16	0.51	2.65	$0.487 + \imath 0.003$	$-0.600 - \imath 0.003$	$-0.121 - \imath 0.001$	$0.623 + \imath 0.003$
(e)	2.33	1.65	1.04	0.08	2.95	$-0.101 + \imath 0.165$	$0.185 - \imath 0.249$	$0.377 + \imath 0.213$	$-0.782 - \imath 0.259$
(f)	0.16	1.41	1.53	0.40	2.46	$-0.715 - \imath 0.001$	$0.661 + \imath 0.023$	$0.015 + \imath 0.106$	$-0.075 - \imath 0.187$
(g)	0.51	2.90	1.08	0.19	1.37	$0.096 + \imath 0.138$	$-0.272 - \imath 0.390$	$-0.103 - \imath 0.148$	$0.482 + \imath 0.693$
(h)	2.52	2.91	0.21	0.25	2.99	$-0.067 + \imath 0.047$	$0.850 - \imath 0.440$	$0.101 + \imath 0.085$	$-0.230 - \imath 0.087$
(i)	1.57	1.38	2.45	0.75	1.41	$0.067 - \imath 0.043$	$-0.072 + \imath 0.047$	$-0.137 + \imath 0.089$	$0.823 - \imath 0.531$
(j)	0.68	2.70	1.01	0.21	0.49	$0.130 - \imath 0.003$	$-0.361 + \imath 0.008$	$-0.072 + \imath 0.002$	$0.920 - \imath 0.021$

Table 2. A numerical estimate of the elements of the down Higgs zero mode eigenvector using the analysis of table 1 and the couplings of eq. (2.3).

Model	a	b_1	b_2	c	$\bar{c}$	$V_{d_{11}}$	$V_{d_{21}}$	$V_{d_{31}}$	$V_{d_{61}}$
(a)	0.22	1.86	1.14	1.46	0.18	-0.273	$0.411 + \imath 0.083$	-0.401	$0.765 + \imath 0.062$
(b)	2.03	2.50	2.70	0.81	1.15	-0.091	0.107	-0.196	0.971
(c)	1.70	2.95	1.21	0.21	2.74	0.323	$-0.783 - \imath 0.010$	0.246	$-0.467 - \imath 0.057$
(d)	0.27	2.55	2.16	0.51	2.65	-0.592	0.708	-0.074	0.378
(e)	2.33	1.65	1.04	0.08	2.95	-0.357	$0.568 + \imath 0.010$	-0.345	$0.644 + \imath 0.127$
(f)	0.16	1.41	1.53	0.40	2.46	0.730	$-0.673 - \imath 0.006$	0.057	$-0.104 - \imath 0.026$
(g)	0.51	2.90	1.08	0.19	1.37	-0.276	0.747	-0.127	0.591
(h)	2.52	2.91	0.21	0.25	2.99	0.086	$-0.977 - \imath 0.055$	0.089	$-0.157 - \imath 0.055$
(i)	1.57	1.38	2.45	0.75	1.41	-0.120	0.095	-0.163	0.975
(j)	0.68	2.70	1.01	0.21	0.49	-0.046	0.163	-0.077	0.983

Table 3. A numerical estimate of the elements of the up Higgs zero mode eigenvector using the analysis of table 1 and the couplings of eq. (2.3).

Model	$f^{(1)}$	$f^{(2)}$	$f^{(3)}$	f^{10_r}
(a)	0.16	0.24	0.03	(0.17, 0.23)
(b)	0.12	0.10	0.12	(0.30, 1.04)
(c)	0.40	0.08	0.08	(2.36, 1.06)
(d)	0.68	0.35	0.22	(0.43, 0.44)
(e)	1.24	0.10	0.04	(0.12, 0.25)
(f)	1.58	0.63	0.10	(2.03, 2.26)
(g)	0.79	0.15	0.14	(0.38, 0.24)
(h)	1.55	0.38	0.22	(1.55, 0.21)
(i)	0.15	0.11	0.08	(1.29, 2.30)
(j)	0.44	0.09	0.22	(0.52, 0.49)

Table 4. The GUT scale parameters in the cubic and quartic superpotentials W_3, $W_4^{(1)}$, $W_4^{(2)}$ and $W_4^{(3)}$ for the model points (a)–(j). The masses are in GeV.

Model	h_t^0	h_b^0	h_τ^0	δh_t^{GUT}	δh_b^{GUT}	$\delta h_\tau^{\text{GUT}}$	h_t^{GUT}	h_b^{GUT}	h_τ^{GUT}
(a)	0.274	0.148	0.148	0.204	0.201	0.063	0.478	0.073	0.088
(b)	0.223	0.238	0.238	0.259	0.282	0.183	0.482	0.044	0.055
(c)	0.190	0.193	0.193	0.319	0.190	0.163	0.501	0.029	0.036
(d)	0.161	0.169	0.169	0.331	0.236	0.089	0.492	0.066	0.081
(e)	0.153	0.278	0.278	0.400	0.341	0.231	0.486	0.062	0.074
(f)	0.189	0.118	0.118	0.298	0.200	0.108	0.484	0.091	0.104
(g)	0.149	0.222	0.222	0.348	0.272	0.159	0.497	0.051	0.062
(h)	0.210	0.198	0.198	0.289	0.220	0.156	0.487	0.042	0.053
(i)	0.268	0.179	0.179	0.216	0.248	0.094	0.483	0.068	0.085
(j)	0.313	0.160	0.160	0.177	0.211	0.099	0.489	0.051	0.060

Table 5. The magnitude of the contributions to the top, bottom, and tau Yukawa couplings from cubic interactions (columns 2–4), from quartic interactions (columns 5–7) and the magnitude of their complex sum (columns 8–10) at the GUT scale for the parameter set of table 4. The Yukawa couplings are in general complex and we add the contributions of the cubic and quartic interactions as complex numbers and exhibit only their magnitudes in the table.

| Model	m_0	A_0	m_1	m_2	m_3	$\tan\beta$	m_t (pole)	$\overline{m}_b(\overline{m}_b)$	m_τ (pole)
(a)	657	-2228	661	526	7774	14.0	172.2	4.15	1.77682
(b)	673	1127	939	570	8833	8.2	172.2	4.22	1.77682
(c)	387	880	949	980	8118	5.3	172.8	4.19	1.77682
(d)	164	197	632	1539	6171	12.2	172.9	4.20	1.77682
(e)	416	339	740	416	4559	11.6	172.8	4.22	1.77682
(f)	688	1450	852	634	8438	16.8	172.9	4.22	1.77682
(g)	106	22.6	523	1309	5240	9.3	172.8	4.19	1.77682
(h)	206	603	842	1298	7510	8.0	172.1	4.15	1.77682
(i)	452	648	624	346	4843	13.1	172.8	4.20	1.77682
(j)	196	-803	828	1599	8929	9.4	172.6	4.22	1.77682

Table 6. The SUGRA parameters sets used for RG analysis where the boundary conditions for the Yukawas for the top, bottom, and the tau are taken from table 5. In the analysis the GUT scale ranges from 8.6×10^{15} GeV to 2.0×10^{16} GeV.

density and of the supersymmetric correction to the muon anomaly is given in table 7. A comparison between table 6 and table 7 shows that one has a unification of Yukawas and a $g-2$ anomaly consistent with the Fermilab result of eq. (1.3). One may note that the dark matter relic density is not fully saturated by the model points of table 7. This implies that the dark matter may likely be multicomponent which includes other forms of dark matter, such as dark fermions of the hidden sector [75–77] or possibly a dark photon [78] or an axion [79, 80].

A scan on the parameter space using the GUT scale input of SO(10) results in a larger set of points than those presented in tables 1–5. The range of values the input parameters take are: $0.5 < \eta, \lambda < 6.0$, $0.1 < a, b_1, b_2, c, \bar{c} < 3.0$, $1 \times 10^{16} < M^{126} < 9.5 \times 10^{17}$, $1 \times 10^{15} < M^{210} < 3.5 \times 10^{16}$, $0.01 < f^{(1)}, f^{(2)}, f^{(3)} < 4.0$ and $0.1 < f^{10_r} < 5.5$. The result of the scan is shown in figure 1. The left panel is a scatter plot in the variables η and λ

Model	h^0	$\tilde{\mu}$	$\tilde{\nu}_\mu$	$\tilde{\tau}$	$\tilde{\chi}_1^0$	$\tilde{\chi}_1^\pm$	Ωh^2	$\Delta a_\mu (\times 10^{-9})$
(a)	123.3	459.0	452.6	270.8	243.1	323.0	0.103	2.30
(b)	125.3	422.8	415.7	370.4	337.3	337.6	0.003	2.14
(c)	123.3	427.2	420.5	379.6	369.8	707.7	0.125	1.91
(d)	123.9	856.4	852.4	243.5	240.1	1227	0.016	1.94
(e)	123.8	361.0	352.6	282.0	272.7	272.9	0.002	1.98
(f)	123.0	508.1	502.3	331.9	324.2	404.3	0.004	2.11
(g)	123.4	722.8	718.2	206.5	195.5	1038.4	0.103	2.57
(h)	124.5	628.7	623.6	338.3	326.8	998.4	0.082	1.94
(i)	123.7	346.8	338.0	240.3	205.6	205.8	0.001	2.67
(j)	123.5	774.1	769.8	319.1	314.7	1247	0.016	2.59

Table 7. Low scale SUSY mass spectrum showing the Higgs boson, the smuon, the muon sneutrino, the stau and the light electroweakino masses and the LSP relic density for the benchmarks of table 6. Also shown is Δa_μ.
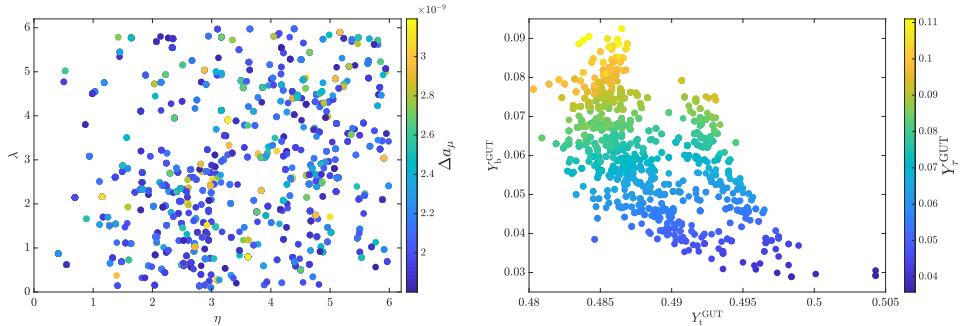

Figure 1. Scatter plots resulting from the scan of input parameters from SO(10). The left panel shows the parameters η and λ with the color axis being the muon $g-2$. The right panel shows the top, bottom and tau Yukawa couplings at the GUT scale.

with the muon $g-2$ shown on the color axis consistent with Δa_μ^{FB}. The right panel shows a scatter plot in the top, bottom and tau Yukawa couplings at the GUT scale. The set of points in the scatter plot is consistent with experimental constraints and the evolution of the GUT scale Yukawas to the electroweak scale produces the correct top, bottom and tau masses within experimental uncertainties.

4 Sparticle hierarchies and signal region analysis

The set of data points retained after satisfying the constraints from the Higgs sector, the DM relic density, dark matter direct detection and the LHC is further processed and points consistent with Yukawa coupling unification are kept. We observe that the spectrum consisting of light electroweakinos, sleptons (selectron and smuons) and staus belong to three cases of mass hierarchy.
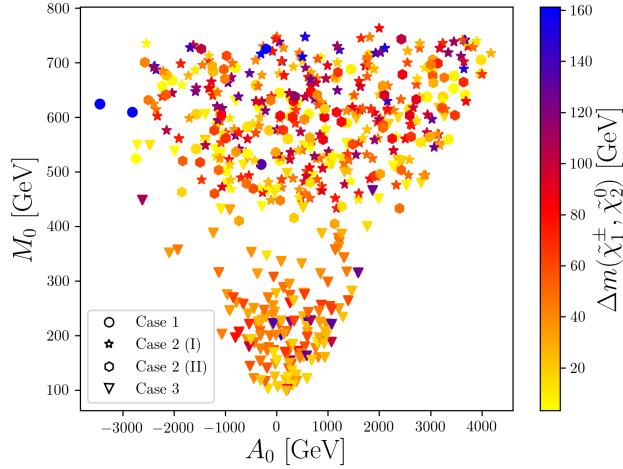
Figure 2. A scatter plot in the M_0-A_0 plane showing the three cases (and subcases) with the chargino-second neutralino mass gap shown on the color axis.

Case 1. The electroweakinos, $\tilde{\chi}_2^0, \tilde{\chi}_1^\pm$ are almost degenerate, with the stau being the next-to-lightest supersymmetric particle (NLSP). The mass hierarchy here is

$$m_{\tilde{\tau}_1} < m_{\widetilde{\mathrm{EW}}} < m_{\tilde{\ell}},$$

where $\widetilde{\mathrm{EW}} = (\tilde{\chi}_2^0, \tilde{\chi}_1^\pm)$ and $\tilde{\ell}$ represents the sleptons.

Case 2. In this category, one of the electroweakinos ($\tilde{\chi}_2^0$ or $\tilde{\chi}_1^\pm$) is the NLSP and the hierarchy reads

$$m_{\widetilde{\mathrm{EW}}} < m_{\tilde{\tau}_1} < m_{\tilde{\ell}}.$$

Here we distinguish two subcategories (I) and (II) where

$$m_{\tilde{\chi}_1^\pm} < m_{\tilde{\chi}_2^0} < m_{\tilde{\tau}_1} \quad (\mathrm{I}),$$
$$m_{\tilde{\chi}_1^\pm} < m_{\tilde{\tau}_1} < m_{\tilde{\chi}_2^0} \quad (\mathrm{II}).$$

Case 3. The last category also includes stau as the NLSP but the electroweakino and slepton hierarchy is inverted, i.e.,

$$m_{\tilde{\tau}_1} < m_{\tilde{\ell}} < m_{\widetilde{\mathrm{EW}}}.$$

Benchmarks (a), (f) belong to Case 1, while (b), (e) and (i) belong to Case 2 and (c), (d), (g), (h) and (j) belong to Case 3. Figure 2 shows the obtained data set categorized according to the above three cases.

An illustration of such a complex spectrum is given in figure 3. The upper panels correspond to benchmark (a) while the lower ones are for (d). Cascade decays are common
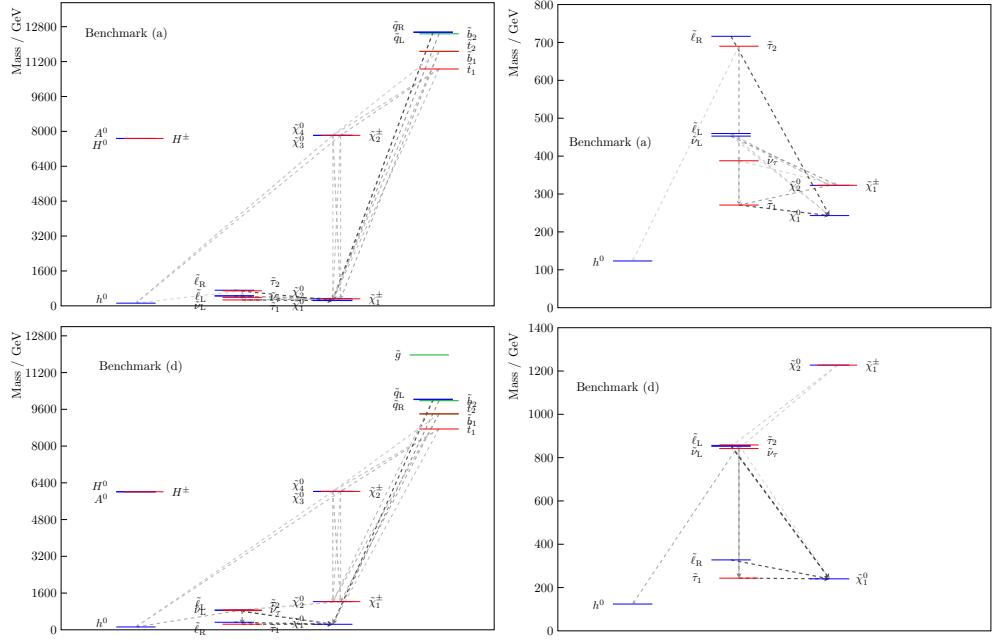
Figure 3. A display of the particle spectrum using `PySLHA` [89] for benchmarks (a) (upper panels) and (d) (lower panels). The left panels represent the spectrum up to 13 TeV while the right panels give the low-lying masses of the spectrum.

in high scale models which, unlike simplified models considered by ATLAS and CMS, produce more complicated event topology. Thus, for slepton pair production, analyses by ATLAS [81, 82] and CMS [83, 84] consider a 100% branching ratio of $\tilde{\ell} \to \ell\tilde{\chi}_1^0$ which can happen in spectra belonging to Case 3. However, Cases 1 and 2 do not necessarily abide by this and one can get several decay channels making the final states more complicated.

In the next section, we select a set of benchmarks belonging to the three cases discussed above. We study slepton pair production and decay at HL-LHC and HE-LHC. We design a set of signal regions to target the rich final states corresponding to the three cases of mass hierarchies. For earlier works on SUSY discovery at HL-LHC and HE-LHC, see refs. [85, 86] and the CERN yellow reports [87, 88].

4.1 Slepton pair production and event simulation at the LHC

The pair production cross section of sleptons (selectrons and smuons) is proportional to the electron and muon Yukawa coupling which means that those cross sections are small compared to staus and electroweak gauginos. For our LHC analysis, we select six of the ten benchmarks shown in table 6 corresponding to sleptons in the mass range of ~ 350 GeV to ~ 850 GeV. The production cross sections of the slepton pairs at 14 TeV and 27 TeV are calculated at the aNNLO+NNLL accuracy using `Resummino-3.0` [90, 91] and the five-flavor NNPDF23NLO PDF set. The results, arranged in decreasing order of cross section, are

Model	$\sigma(pp \to \tilde{e}_L\,\tilde{e}_L)$		$\sigma(pp \to \tilde{\mu}_L\,\tilde{\mu}_L)$		Branching ratios		
	14 TeV	27 TeV	14 TeV	27 TeV	$\tilde{\ell}_L \to \ell\tilde{\chi}_1^0$	$\tilde{\ell}_L \to \ell\tilde{\chi}_2^0$	$\tilde{\ell}_L \to \nu_\ell\tilde{\chi}_1^\pm$
(i)	2.896	9.633	2.909	9.673	31%	6%	63%
(b)	1.242	4.590	1.244	4.598	31%	6%	63%
(f)	0.541	2.252	0.543	2.262	22%	26%	52%
(h)	0.194	0.958	0.194	0.957	100%	-	-
(g)	0.094	0.533	0.094	0.533	100%	-	-
(d)	0.037	0.253	0.037	0.253	100%	-	-

Table 8. The aNNLO+NNLL pair production cross-sections, in fb, of sleptons at $\sqrt{s} = 14\,\text{TeV}$ and at $\sqrt{s} = 27\,\text{TeV}$ for benchmarks (b), (d) and (f)–(i) of table 1 arranged in decreasing order of production cross sections. Also shown are the slepton branching ratios to electroweakinos and leptons.

shown in table 8. Also shown are the different branching ratios of sleptons but for brevity we do not exhibit the branching ratios of $\tilde{\chi}_2^0$ and $\tilde{\chi}_1^\pm$ for benchmarks (b), (f) and (i). To have an idea of the decay channels involved, one can examine the right panel of figure 3 which shows the low-lying spectrum of benchmark (a). Since (a) and (f) both belong to Case 1, one can have an idea of the different decay channels of $\tilde{\chi}_2^0$ and $\tilde{\chi}_1^\pm$ which involve the stau. This leads to a tau-enriched final state.

The final states which make up our signal region (SR) involve two same flavor and opposite sign (SFOS) leptons with missing transverse energy (MET). We also require at least two jets (N $\geq$ 2) which can be used to form kinematic variables that are effective for jetty final states. We call the signal region SR-2ℓNj. For such final states, the dominant SM backgrounds are from diboson production, Z/γ+jets, dilepton production from off-shell vector bosons ($V^* \to \ell\ell$), $t\bar{t}$ and $t + W/Z$. The subdominant backgrounds are Higgs production via gluon fusion (ggF H) and vector boson fusion (VBF). The simulation of the signal and background events is performed at LO with `MadGraph5_aMC@NLO-3.1.0` interfaced to `LHAPDF` [92] using the NNPDF30LO PDF set. Up to two hard jets are added at generator level. The parton level events are passed to `PYTHIA8` [93] for showering and hadronization using a five-flavor matching scheme in order to avoid double counting of jets. For the signal events, the matching/merging scale is set at one-fourth the mass of the pair produced sleptons. Additional jets from ISR and FSR are added to the signal and background events. Jets are clustered with `FastJet` [94] using the anti-k_t algorithm [95] with jet radius $R = 0.4$. `DELPHES-3.4.2` [96] is then employed for detector simulation and event reconstruction using the HL-LHC and HE-LHC card. The SM backgrounds are scaled to their relevant NLO cross sections while aNNLO+NNLL cross sections are used for the signal events.

4.2 Event selection

The selected SFOS leptons must have a leading and subleading transverse momenta $p_T > 15\,\text{GeV}$ for electrons and $p_T > 10\,\text{GeV}$ for muons with $|\eta| < 2.5$. Each event should contain at least two non-b-tagged jets with the leading $p_T > 20\,\text{GeV}$ in the $|\eta| < 2.4$ region and

a missing transverse energy $E_T^{\text{miss}} > 70\,\text{GeV}$. Despite the specific preselection criteria, the analysis cuts used for the six benchmarks cannot be the same. This is due to the rich final states involved. To help us discriminate the signal from the background events, we use a set of kinematic variables along with a deep neural network (DNN) which is trained and tested on two independent sets of signal and background samples. We list the kinematic variables that enter in the training of the DNN:

1. E_T^{miss}: the missing transverse energy in the event. It is usually high for the signal due to the presence of neutralinos.

2. The transverse momentum of the leading non-b tagged jets, $p_T(j_1)$. Rejecting b-tagged jets reduces the $t\bar{t}$ background.

3. The transverse momentum of the leading lepton (electron or muon), $p_T(\ell_1)$.

4. M_{T2}, the stransverse mass [97–99] of the leading and subleading leptons

$$M_{\text{T2}} = \min\left[\max\left(m_{\text{T}}(\mathbf{p}_{\text{T}}^{\ell_1}, \mathbf{q}_{\text{T}}), m_{\text{T}}(\mathbf{p}_{\text{T}}^{\ell_2}, \mathbf{p}_{\text{T}}^{\text{miss}} - \mathbf{q}_{\text{T}})\right)\right], \qquad (4.1)$$

where $\mathbf{q}_{\text{T}}$ is an arbitrary vector chosen to find the appropriate minimum and the transverse mass m_T is given by

$$m_{\text{T}}(\mathbf{p}_{\text{T1}}, \mathbf{p}_{\text{T2}}) = \sqrt{2(p_{\text{T1}}\, p_{\text{T2}} - \mathbf{p}_{\text{T1}} \cdot \mathbf{p}_{\text{T2}})}. \qquad (4.2)$$

5. The quantity $M_{\text{T}}^{\text{min}}$ defined as $M_{\text{T}}^{\text{min}} = \min[m_{\text{T}}(\mathbf{p}_{\text{T}}^{\ell_1}, \mathbf{p}_{\text{T}}^{\text{miss}}), m_{\text{T}}(\mathbf{p}_{\text{T}}^{\ell_2}, \mathbf{p}_{\text{T}}^{\text{miss}})]$. The variables M_{T2} and $M_{\text{T}}^{\text{min}}$ are effective when dealing with large MET in the final state.

6. The dilepton invariant mass, $m_{\ell\ell}$, helps in rejecting the diboson background with a peak near the Z boson mass which can be done by setting $m_{\ell\ell} > 100\,\text{GeV}$.

7. The opening angle between the MET system and the dilepton system, $\Delta\phi(\mathbf{p}_{\text{T}}^{\ell}, \mathbf{p}_{\text{T}}^{\text{miss}})$, where $\mathbf{p}_{\text{T}}^{\ell} = \mathbf{p}_{\text{T}}^{\ell_1} + \mathbf{p}_{\text{T}}^{\ell_2}$.

8. The smallest opening angle between the first three leading jets in an event and the MET system, $\Delta\phi_{\text{min}}(\mathbf{p}_{\text{T}}(j_i), \mathbf{p}_{\text{T}}^{\text{miss}})$, where $i = 1, 2, 3$.

We use the DNN implementation in the 'Toolkit for Multivariate Analysis' (TMVA) [100] framework within ROOT6 [101]. The DNN employed has three dense hidden layers with 128 neurons per layer and tanh as an activation function to define the output neurons given the input values. The DNN trains on the signal and background events using the above set of kinematic variables in three phases with a decreasing learning rate. After the 'learning' process is over, the DNN tests the predictions on another set of signal and background samples. Despite having one background set, the training and testing must be done every time a signal sample is used, i.e., six times in our case. During the testing stage, the DNN creates a new discriminator which is called the DNN response or the DNN score. Cuts on this new variable maximizes the signal (S) to background (B) ratio, $S/\sqrt{S+B}$.

Variable	(b), (i)	(f)	(d), (g), (h)
$m_{\ell\ell}$ [GeV] $>$	136 (110)	150	150 (110)
$E_T^{\mathrm{miss}}/\mathbf{p}_T^{\ell} >$	1.9 (2.8)	-	-
$\Delta\phi_{\min}(\mathbf{p}_{\mathrm{T}}(j_i), \mathbf{p}_{\mathrm{T}}^{\mathrm{miss}})$ [rad] $>$	-	0.85 (1.5)	-
$p_T^{\ell_2}$ [GeV] $>$	-	-	190 (370)
M_{T2} [GeV] $>$	- (140)	- (120)	200 (300)
DNN response $>$	0.9	0.9	0.9
$\mathcal{L}$ at 14 TeV [fb^{-1}]	NV, 1887	1262	NV, 2074, 1738
$\mathcal{L}$ at 27 TeV [fb^{-1}]	2804, 1320	694	1031, 689, 1194

Table 9. The analysis cuts on a set of kinematic variables at 14 TeV (27 TeV) grouped by the benchmarks of table 6. Notice that with the exception of $m_{\ell\ell}$ harder cuts are applied at 27 TeV. Entries with a dash (-) mean that no requirement on the variable is considered. Also shown at the bottom are the required integrated luminosities for discovery at 14 TeV and 27 TeV. Entries with 'NV' mean that the point is not visible at the corresponding center-of-mass energy.

We give in table 9 the set of analysis cuts on a select number of kinematic variables along with the new 'DNN response' variable. Variations in cuts are used for our six benchmarks depending on the hierarchy of the spectrum which allows us to put them in three categories with (b),(i) as the first, (f) as the second and (d),(g),(h) as the third. The values shown in parentheses are the modified cuts at 27 TeV which are essential to improving the $S/\sqrt{S+B}$ ratio.

4.3 Results

We begin by discussing the benchmarks (d), (g) and (h) which belong to Case 3. Here the mass splitting between the slepton and the neutralino is large, ranging from 300 GeV to 600 GeV, which produces very energetic leptons. For those benchmarks, the sleptons decay to a light lepton and a neutralino with a 100% branching ratio (see table 8) which makes for a clean final state. The most effective kinematic variables for this case are M_{T2} and $p_T^{\ell_2}$ where the latter is the transverse momentum of the subleading lepton. We present two-dimensional plots in these variables in the middle panels of figure 4. The left panel depicts point (d) and the right one is the dominant diboson background. One can clearly see that the largest number of background events (color axis) are concentrated at small M_{T2} and $p_T^{\ell_2}$ while for the signal larger values are highly populated as well due to the energetic final states. A hard cut on M_{T2} and $p_T^{\ell_2}$ as well as the 'DNN response' can reject most of the background events.

Next, we discuss benchmarks (b) and (i) which belong to Case 2. Here the branching ratios to a lepton and a neutralino are smaller, at 31% and the slepton-neutralino mass gaps are at 85 GeV and 140 GeV, respectively. Such a mass gap is not enough to allow harder cuts on $p_T^{\ell_2}$ and that's why it has been omitted in table 9. For this reason, we make use of the leading and subleading transverse momenta of the leptons to reconstruct the total momentum of the system, $\mathbf{p}_{\mathrm{T}}^{\ell}$, to form the new variable $E_T^{\mathrm{miss}}/\mathbf{p}_{\mathrm{T}}^{\ell}$. Two-dimensional
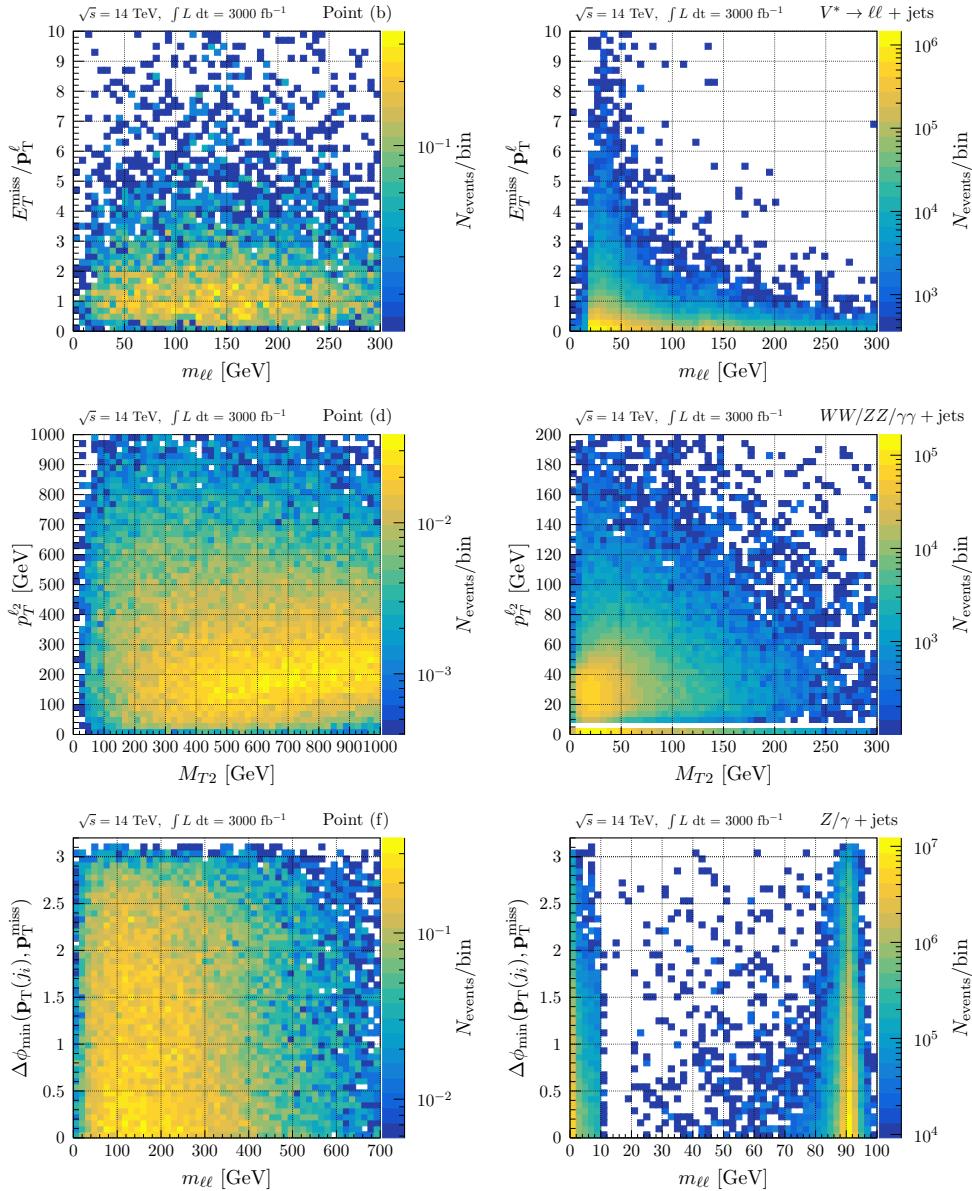
Figure 4. Two dimensional plots in select kinematic variables with the number of events on the color axis. Top panels: $E_T^{\text{miss}}/\mathbf{p}_T^\ell$ vs the dilepton invariant mass for benchmark (b) (left) and off-shell vector boson background (right). Middle panels: the subleading lepton transverse momentum vs M_{T2} for benchmark (d) (left) and the diboson background (right). Bottom panels: $\Delta\phi_{\text{min}}(\mathbf{p}_T(j_i), \mathbf{p}_T^{\text{miss}})$ vs the dilepton invariant mass for benchmark (f) (left) and Z/γ + jets background (right).
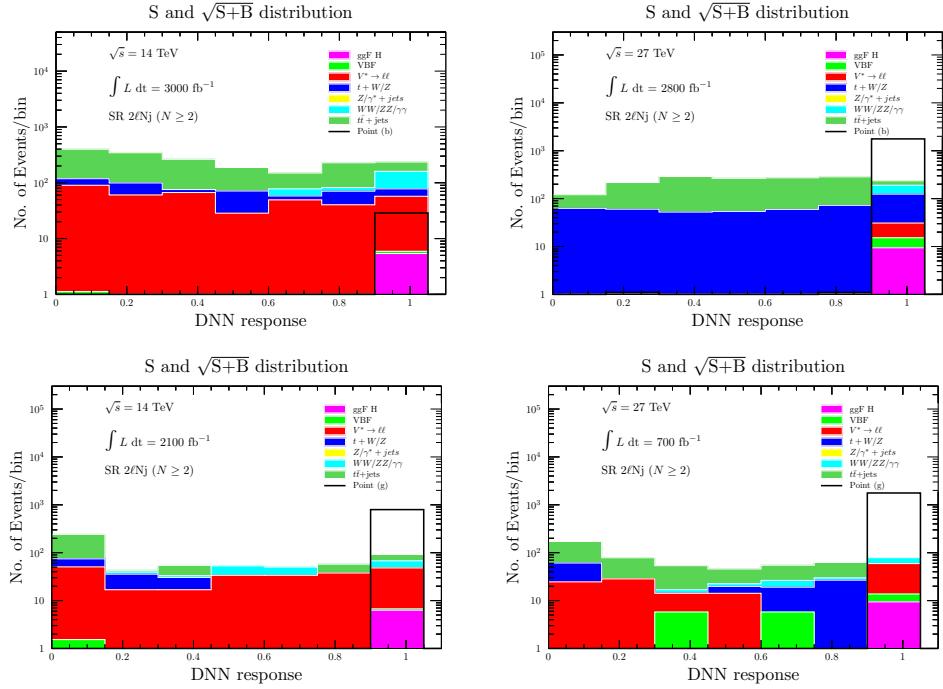
Figure 5. Distributions in the DNN response variable at 14 TeV (left) and 27 TeV (right) for benchmarks (b) (top panels) and (g) (bottom panels).

plots in the $E_T^{\mathrm{miss}}/\mathbf{p}_T^\ell$ and the dilepton invariant mass, $m_{\ell\ell}$, variables are shown in the top panels of figure 4. The left panel shows the distributions for point (b) while the right one is for dilepton production from off-shell vector bosons. For the background, most of the events lie in the region $E_T^{\mathrm{miss}}/\mathbf{p}_T^\ell < 2$ and $m_{\ell\ell} < 100\,\mathrm{GeV}$ which is the reason for the choice of cuts in table 9.

Finally, for point (f) which belongs to Case 1, the branching fraction to a lepton and a neutralino is the smallest compared to its decay to a second neutralino and a chargino. The second neutralino and chargino decay predominantly to a stau which in turn decays to a neutralino and a tau. Hence we are faced with a case of tau-enriched final state which can hadronize forming jets. In our selection, we have rejected b-tagged jets but made no special requirements on tau-tagged jets. For this particular case, jets (tau-tagged or not) can be used to reject the SM background through the variable $\Delta\phi_{\min}(\mathbf{p}_T(j_i), \mathbf{p}_T^{\mathrm{miss}})$ defined above. In the bottom panels of figure 4 we show this variable plotted against $m_{\ell\ell}$ for point (f) (left panel) and the Z/γ+jets background (right panel). Excluding the region formed by $\Delta\phi_{\min}(\mathbf{p}_T(j_i), \mathbf{p}_T^{\mathrm{miss}}) < 1$ rad and $m_{\ell\ell} < 100\,\mathrm{GeV}$ is effective in reducing the SM background.

Along with cuts on the variables discussed thus far, the 'DNN response' plays an important role. We show in figure 5 distributions in this variable after the above cuts have been implemented. The top panel depicts benchmark (b) which shows clearly that

at 14 TeV this point cannot be discovered with $3000\,\mathrm{fb}^{-1}$ while the signal is in excess over the background near 1 for $2800\,\mathrm{fb}^{-1}$ at 27 TeV. The bottom panels show point (g) also at 14 TeV (left) and 27 TeV (right). The benchmark is discoverable at both HL-LHC and HE-LHC but requires smaller integrated luminosity for discovery at HE-LHC ($700\,\mathrm{fb}^{-1}$) than at HL-LHC ($2100\,\mathrm{fb}^{-1}$). The evaluated integrated luminosities for discovery at both machines are summarized in the lower part of table 9. Entries with 'NV' indicate that the benchmark is not discoverable at the corresponding machine. Note that there is a modest improvement in the integrated luminosity at HE-LHC in comparison to HL-LHC but the former is expected to gather data at the rate of $\sim 820\,\mathrm{fb}^{-1}$ per month, so most of those points will be discoverable within the first two to three months of run. Note that points (f), (g), (h) and (i) are discoverable at both machines while (b) and (d) can only be discoverable at HE-LHC.

We note that recently several works have come out regarding a SUSY explanation of the Fermilab muon $g - 2$ [102–118].

5 Conclusion

In this work we have investigated if high scale models can produce Yukawa coupling unification consistent with the Fermilab muon $g - 2$ result. We used a neural network to investigate the parameter space of a class of $SO(10)$ models where Yukawa couplings arise from the cubic as well as the quartic interactions. As in a recent work it is found that the preferred parameter space lies in a region where gluino-driven radiative breaking of the electroweak symmetry occurs. The model produces a split spectrum consisting of a light sector and a heavy sector. The light sector contains light sleptons and light weakinos, and the heavy sector contains the gluino, the squarks and the heavy Higgs. The masses of the light sparticles lie in the few hundred GeV range and are accessible at the LHC. With the help of a deep neural network, we carried out a dedicated search of sleptons in the two-lepton final state at HL-LHC and HE-LHC. It is found that most of the considered benchmarks are discoverable within the optimal integrated luminosity of HL-LHC while all of them are discoverable at HE-LHC with less integrated luminosities.

Acknowledgments

A Contributions to Yukawas from higher dimensional operators

In this appendix we give the contributions $\delta h_b, \delta h_t, \delta h_\tau$ to the Yukawas that arise from higher dimensional operators where

$$\delta h_t = \delta h_t^{(1)} + \delta h_t^{(2)} + \delta h_t^{(3)}, \quad \delta h_b = \delta h_b^{(1)} + \delta h_b^{(2)} + \delta h_b^{(3)}, \quad \delta h_\tau = \delta h_\tau^{(1)} + \delta h_\tau^{(2)} + \delta h_\tau^{(3)}. \tag{A.1}$$

Here $\delta h^{(1)}$ is the contribution arising from $W_4^{(1)}$, $\delta h^{(2)}$ is the contribution arising from $W_4^{(2)}$, and $\delta h^{(3)}$ is the contribution arising from $W_4^{(3)}$. The explicit forms of these are given below [9].

Thus $W_4^{(1)}$ gives the following contribution to the third generation Yukawas

$$\delta h_t^{(1)} = \frac{if^{(1)}}{60\sqrt{2}M_c}\left(\sum_{r=1}^{2} b_r U_{d_{r1}}\right)\left[\frac{5\sqrt{3}}{2}\mathcal{V}_{75_{210}} - 4\sqrt{15}\mathcal{V}_{24_{210}} - 8\sqrt{15}\mathcal{V}_{1_{210}}\right], \quad \text{(A.2)}$$

$$\delta h_b^{(1)} = \frac{if^{(1)}}{60\sqrt{2}M_c}\left(\sum_{r=1}^{2} b_r V_{d_{r1}}\right)\left[\frac{\sqrt{20}}{3}\mathcal{V}_{75_{210}} - 20\sqrt{\frac{5}{3}}\mathcal{V}_{24_{210}}\right], \quad \text{(A.3)}$$

$$\delta h_\tau^{(1)} = \frac{if^{(1)}}{60\sqrt{2}M_c}\left(\sum_{r=1}^{2} b_r V_{d_{r1}}\right)\left[20\sqrt{3}\mathcal{V}_{75_{210}} - 20\sqrt{15}\mathcal{V}_{24_{210}}\right], \quad \text{(A.4)}$$

The contribution of $W_4^{(2)}$ to the third generation Yukawas is given by

$$\delta h_t^{(2)} = -\frac{if^{(2)}}{120M_c}\left[\frac{10}{3}\sqrt{\frac{2}{3}}\mathcal{V}_{75_{210}}U_{d_{61}} + \frac{5}{3}\sqrt{\frac{10}{3}}\mathcal{V}_{24_{210}}U_{d_{61}} + 6\sqrt{5}\mathcal{V}_{24_{210}}U_{d_{31}} - 8\sqrt{5}\mathcal{V}_{1_{210}}U_{d_{31}}\right],$$
$$\text{(A.5)}$$

$$\delta h_b^{(2)} = -\frac{if^{(2)}}{120M_c}\left[-\frac{20}{3}\sqrt{\frac{2}{3}}\mathcal{V}_{75_{210}}V_{d_{61}} - \frac{20}{3}\mathcal{V}_{75_{210}}V_{d_{31}} - \frac{1}{3}\sqrt{\frac{10}{3}}\mathcal{V}_{24_{210}}V_{d_{61}} - \frac{10\sqrt{5}}{3}\mathcal{V}_{24_{210}}V_{d_{31}}\right.$$
$$\left.- 4\sqrt{\frac{10}{3}}\mathcal{V}_{1_{210}}V_{d_{61}}\right], \quad \text{(A.6)}$$

$$\delta h_\tau^{(2)} = -\frac{if^{(2)}}{120M_c}\left[-20\sqrt{\frac{2}{3}}\mathcal{V}_{75_{210}}V_{d_{61}} - 20\mathcal{V}_{75_{210}}V_{d_{31}} - \sqrt{\frac{10}{3}}\mathcal{V}_{24_{210}}V_{d_{61}} - 10\sqrt{5}\mathcal{V}_{24_{210}}V_{d_{31}}\right.$$
$$\left.- 4\sqrt{30}\mathcal{V}_{1_{210}}V_{d_{61}}\right]. \quad \text{(A.7)}$$

Finally, the contribution of $W_4^{(3)}$ to the third generation Yukawas is given by

$$\delta h_t^{(3)} = -\frac{3i}{8}\frac{f^{(3)}}{M_c}\left[\frac{2}{3}\sqrt{\frac{2}{3}}\mathcal{V}_{75_{210}}U_{d_{61}} + \frac{1}{3}\sqrt{\frac{10}{3}}\mathcal{V}_{24_{210}}U_{d_{61}} - \frac{2}{\sqrt{5}}\mathcal{V}_{24_{210}}U_{d_{31}} + \frac{8}{3\sqrt{5}}\mathcal{V}_{1_{210}}U_{d_{31}}\right],$$
$$\text{(A.8)}$$

$$\delta h_b^{(3)} = -\frac{3i}{8}\frac{f^{(3)}}{M_c}\left[\frac{2}{3}\sqrt{\frac{2}{3}}\mathcal{V}_{75_{210}}V_{d_{61}} + \frac{1}{3}\sqrt{\frac{10}{3}}\mathcal{V}_{24_{210}}V_{d_{61}} - \frac{2}{\sqrt{5}}\mathcal{V}_{24_{210}}V_{d_{31}} + \frac{8}{3\sqrt{5}}\mathcal{V}_{1_{210}}V_{d_{31}}\right],$$
$$\text{(A.9)}$$

$$\delta h_\tau^{(3)} = \frac{3i}{8}\frac{f^{(3)}}{M_c}\left[\frac{2}{3}\sqrt{\frac{2}{3}}\mathcal{V}_{75_{210}}V_{d_{61}} + \frac{1}{3}\sqrt{\frac{10}{3}}\mathcal{V}_{24_{210}}V_{d_{61}} - \frac{2}{\sqrt{5}}\mathcal{V}_{24_{210}}V_{d_{31}} + \frac{8}{3\sqrt{5}}\mathcal{V}_{1_{210}}V_{d_{31}}\right].$$
$$\text{(A.10)}$$

The total Yukawas are the sum of the contributions from the cubic and from the quartic terms at the GUT scale as given in eq. (2.12).

References

[1] Muon g-2 collaboration, *Measurement of the Positive Muon Anomalous Magnetic Moment to 0.46 ppm*, *Phys. Rev. Lett.* **126** (2021) 141801 [`arXiv:2104.03281`] [INSPIRE].

[2] Muon g-2 collaboration, *Final Report of the Muon E821 Anomalous Magnetic Moment Measurement at BNL*, *Phys. Rev. D* **73** (2006) 072003 [`hep-ex/0602035`] [INSPIRE].

[3] Particle Data Group collaboration, *Review of Particle Physics*, *Phys. Rev. D* **98** (2018) 030001 [INSPIRE].

[4] T. Aoyama et al., *The anomalous magnetic moment of the muon in the Standard Model*, *Phys. Rept.* **887** (2020) 1 [`arXiv:2006.04822`] [INSPIRE].

[5] S. Borsanyi et al., *Leading hadronic contribution to the muon magnetic moment from lattice QCD*, *Nature* **593** (2021) 51 [`arXiv:2002.12347`] [INSPIRE].

[6] A. Aboubrahim, M. Klasen and P. Nath, *What Fermilab $(g-2)_\mu$ experiment tells us about discovering SUSY at HL-LHC and HE-LHC*, `arXiv:2104.03839` [INSPIRE].

[7] S. Akula and P. Nath, *Gluino-driven radiative breaking, Higgs boson mass, muon g-2, and the Higgs diphoton decay in supergravity unification*, *Phys. Rev. D* **87** (2013) 115022 [`arXiv:1304.5526`] [INSPIRE].

[8] A. Aboubrahim and P. Nath, *Mixed hidden sector-visible sector dark matter and observation of a CP odd Higgs boson at HL-LHC and HE-LHC*, *Phys. Rev. D* **100** (2019) 015042 [`arXiv:1905.04601`] [INSPIRE].

[9] A. Aboubrahim, P. Nath and R.M. Syed, *Corrections to Yukawa couplings from higher dimensional operators in a natural SUSY* SO(10) *and HL-LHC implications*, *JHEP* **01** (2021) 047 [`arXiv:2005.00867`] [INSPIRE].

[10] K.S. Babu, I. Gogoladze and Z. Tavartkiladze, *Missing Partner Mechanism in* SO(10) *Grand Unification*, *Phys. Lett. B* **650** (2007) 49 [`hep-ph/0612315`] [INSPIRE].

[11] K.S. Babu, I. Gogoladze, P. Nath and R.M. Syed, *Variety of* SO(10) *GUTs with Natural Doublet-Triplet Splitting via the Missing Partner Mechanism*, *Phys. Rev. D* **85** (2012) 075002 [`arXiv:1112.5387`] [INSPIRE].

[12] A. Masiero, D.V. Nanopoulos, K. Tamvakis and T. Yanagida, *Naturally Massless Higgs Doublets in Supersymmetric* SU(5), *Phys. Lett. B* **115** (1982) 380 [INSPIRE].

[13] B. Grinstein, *A Supersymmetric* SU(5) *Gauge Theory with No Gauge Hierarchy Problem*, *Nucl. Phys. B* **206** (1982) 387 [INSPIRE].

[14] T.E. Clark, T.-K. Kuo and N. Nakagawa, *A* SO(10) *supersymmetric grand unified theory*, *Phys. Lett. B* **115** (1982) 26 [INSPIRE].

[15] C.S. Aulakh and R.N. Mohapatra, *Implications of Supersymmetric* SO(10) *Grand Unification*, *Phys. Rev. D* **28** (1983) 217 [INSPIRE].

[16] K.S. Babu and R.N. Mohapatra, *Predictive neutrino spectrum in minimal* SO(10) *grand unification*, *Phys. Rev. Lett.* **70** (1993) 2845 [`hep-ph/9209215`] [INSPIRE].

– 19 –

[17] P. Nath and R.M. Syed, *Analysis of couplings with large tensor representations in* SO(2N) *and proton decay*, *Phys. Lett. B* **506** (2001) 68 [*Erratum ibid.* **508** (2001) 216] [hep-ph/0103165] [INSPIRE].

[18] P. Nath and R.M. Syed, *Complete cubic and quartic couplings of 16 and bar-16 in* SO(10) *unification*, *Nucl. Phys. B* **618** (2001) 138 [hep-th/0109116] [INSPIRE].

[19] P. Nath and R.M. Syed, *Coupling the supersymmetric 210 vector multiplet to matter in* SO(10), *Nucl. Phys. B* **676** (2004) 64 [hep-th/0310178] [INSPIRE].

[20] C.S. Aulakh, B. Bajc, A. Melfo, G. Senjanović and F. Vissani, *The Minimal supersymmetric grand unified theory*, *Phys. Lett. B* **588** (2004) 196 [hep-ph/0306242] [INSPIRE].

[21] B. Bajc, A. Melfo, G. Senjanović and F. Vissani, *The Minimal supersymmetric grand unified theory. 1. Symmetry breaking and the particle spectrum*, *Phys. Rev. D* **70** (2004) 035007 [hep-ph/0402122] [INSPIRE].

[22] C.S. Aulakh and A. Girdhar, SO(10) *MSGUT: Spectra, couplings and threshold effects*, *Nucl. Phys. B* **711** (2005) 275 [hep-ph/0405074] [INSPIRE].

[23] C.S. Aulakh and S.K. Garg, *The New Minimal Supersymmetric GUT: Spectra, RG analysis and Fermion Fits*, *Nucl. Phys. B* **857** (2012) 101 [arXiv:0807.0917] [INSPIRE].

[24] P. Nath and P. Fileviez Perez, *Proton stability in grand unified theories, in strings and in branes*, *Phys. Rept.* **441** (2007) 191 [hep-ph/0601023] [INSPIRE].

[25] D.A. Kosower, L.M. Krauss and N. Sakai, *Low-Energy Supergravity and the Anomalous Magnetic Moment of the Muon*, *Phys. Lett. B* **133** (1983) 305 [INSPIRE].

[26] T.C. Yuan, R.L. Arnowitt, A.H. Chamseddine and P. Nath, *Supersymmetric Electroweak Effects on G-2 (mu)*, *Z. Phys. C* **26** (1984) 407 [INSPIRE].

[27] J.L. Lopez, D.V. Nanopoulos and X. Wang, *Large (g-2)-mu in* SU(5) × U(1) *supergravity models*, *Phys. Rev. D* **49** (1994) 366 [hep-ph/9308336] [INSPIRE].

[28] U. Chattopadhyay and P. Nath, *Probing supergravity grand unification in the Brookhaven g-2 experiment*, *Phys. Rev. D* **53** (1996) 1648 [hep-ph/9507386] [INSPIRE].

[29] T. Moroi, *The Muon anomalous magnetic dipole moment in the minimal supersymmetric standard model*, *Phys. Rev. D* **53** (1996) 6565 [*Erratum ibid.* **56** (1997) 4424] [hep-ph/9512396] [INSPIRE].

[30] M. Carena, G.F. Giudice and C.E.M. Wagner, *Constraints on supersymmetric models from the muon anomalous magnetic moment*, *Phys. Lett. B* **390** (1997) 234 [hep-ph/9610233] [INSPIRE].

[31] A. Czarnecki and W.J. Marciano, *The Muon anomalous magnetic moment: A Harbinger for 'new physics'*, *Phys. Rev. D* **64** (2001) 013014 [hep-ph/0102122] [INSPIRE].

[32] U. Chattopadhyay and P. Nath, *Upper limits on sparticle masses from g-2 and the possibility for discovery of SUSY at colliders and in dark matter searches*, *Phys. Rev. Lett.* **86** (2001) 5854 [hep-ph/0102157] [INSPIRE].

[33] L.L. Everett, G.L. Kane, S. Rigolin and L.-T. Wang, *Implications of muon g-2 for supersymmetry and for discovering superpartners directly*, *Phys. Rev. Lett.* **86** (2001) 3484 [hep-ph/0102145] [INSPIRE].

[34] J.L. Feng and K.T. Matchev, *Supersymmetry and the anomalous magnetic moment of the muon*, *Phys. Rev. Lett.* **86** (2001) 3480 [hep-ph/0102146] [INSPIRE].

[35] E.A. Baltz and P. Gondolo, *Implications of muon anomalous magnetic moment for supersymmetric dark matter*, *Phys. Rev. Lett.* **86** (2001) 5004 [hep-ph/0102147] [INSPIRE].

[36] D. Sabatta, A.S. Cornell, A. Goyal, M. Kumar, B. Mellado and X. Ruan, *Connecting muon anomalous magnetic moment and multi-lepton anomalies at LHC*, *Chin. Phys. C* **44** (2020) 063103 [arXiv:1909.03969] [INSPIRE].

[37] S. Buddenbrock et al., *The emergence of multi-lepton anomalies at the LHC and their compatibility with new physics at the EW scale*, *JHEP* **10** (2019) 157 [arXiv:1901.05300] [INSPIRE].

[38] N. Chen, B. Wang and C.-Y. Yao, *The collider tests of a leptophilic scalar for the anomalous magnetic moments*, arXiv:2102.05619 [INSPIRE].

[39] A. Crivellin, M. Hoferichter, *Consequences of chirally enhanced explanations of $(g-2)_\mu$ for $h \to \mu\mu$ and $Z \to \mu\mu$*, arXiv:2104.03202 [INSPIRE].

[40] E. Coluccio Leskow, A. Crivellin, G. D'Ambrosio and D. Müller, *$(g-2)_\mu$, Lepton Flavour Violation and Z Decays with Leptoquarks: Correlations and Future Prospects*, *Phys. Rev. D* **95** (2017) 055018 [arXiv:1612.06858] [INSPIRE].

[41] S. Akula, B. Altunkaynak, D. Feldman, P. Nath and G. Peim, *Higgs Boson Mass Predictions in SUGRA Unification, Recent LHC-7 Results, and Dark Matter*, *Phys. Rev. D* **85** (2012) 075001 [arXiv:1112.3645] [INSPIRE].

[42] A. Arbey, M. Battaglia, A. Djouadi, F. Mahmoudi and J. Quevillon, *Implications of a 125 GeV Higgs for supersymmetric models*, *Phys. Lett. B* **708** (2012) 162 [arXiv:1112.3028] [INSPIRE].

[43] H. Baer, V. Barger and A. Mustafayev, *Implications of a 125 GeV Higgs scalar for LHC SUSY and neutralino dark matter searches*, *Phys. Rev. D* **85** (2012) 075010 [arXiv:1112.3017] [INSPIRE].

[44] J. Ellis and K.A. Olive, *Revisiting the Higgs Mass and Dark Matter in the CMSSM*, *Eur. Phys. J. C* **72** (2012) 2005 [arXiv:1202.3262] [INSPIRE].

[45] S. Heinemeyer, O. Stal and G. Weiglein, *Interpreting the LHC Higgs Search Results in the MSSM*, *Phys. Lett. B* **710** (2012) 201 [arXiv:1112.3026] [INSPIRE].

[46] B. Ananthanarayan, G. Lazarides and Q. Shafi, *Radiative electroweak breaking and sparticle spectroscopy with tan Beta approximately = m(t) / m(b)*, *Phys. Lett. B* **300** (1993) 245 [INSPIRE].

[47] U. Chattopadhyay, A. Corsetti and P. Nath, *Supersymmetric dark matter and Yukawa unification*, *Phys. Rev. D* **66** (2002) 035003 [hep-ph/0201001] [INSPIRE].

[48] J. Hollingsworth, M. Ratz, P. Tanedo and D. Whiteson, *Efficient sampling of constrained high-dimensional theoretical spaces with machine learning*, arXiv:2103.06957 [INSPIRE].

[49] DARKMACHINES HIGH DIMENSIONAL SAMPLING GROUP collaboration, *A comparison of optimisation algorithms for high-dimensional particle and astrophysics applications*, *JHEP* **05** (2021) 108 [arXiv:2101.04525] [INSPIRE].

[50] A.H. Chamseddine, R.L. Arnowitt and P. Nath, *Locally Supersymmetric Grand Unification*, *Phys. Rev. Lett.* **49** (1982) 970 [INSPIRE].

[51] P. Nath, R.L. Arnowitt and A.H. Chamseddine, *Gauge Hierarchy In Supergravity Guts*, *Nucl. Phys. B* **227** (1983) 121 [INSPIRE].

[52] L.J. Hall, J.D. Lykken and S. Weinberg, *Supergravity as the Messenger of Supersymmetry Breaking*, *Phys. Rev. D* **27** (1983) 2359 [INSPIRE].

[53] P. Nath, R.L. Arnowitt and A.H. Chamseddine, *Model independent analysis of low-energy phenomena in supergravity unified theories*, HUTP-83/A077.

[54] J.R. Ellis, K. Enqvist, D.V. Nanopoulos and K. Tamvakis, *Gaugino Masses and Grand Unification*, *Phys. Lett. B* **155** (1985) 381 [INSPIRE].

[55] A. Corsetti and P. Nath, *Gaugino mass nonuniversality and dark matter in SUGRA, strings and D-brane models*, *Phys. Rev. D* **64** (2001) 125010 [hep-ph/0003186] [INSPIRE].

[56] A. Birkedal-Hansen and B.D. Nelson, *Relic neutralino densities and detection rates with nonuniversal gaugino masses*, *Phys. Rev. D* **67** (2003) 095006 [hep-ph/0211071] [INSPIRE].

[57] G. Bélanger, F. Boudjema, A. Cottrant, A. Pukhov and A. Semenov, *WMAP constraints on SUGRA models with non-universal gaugino masses and prospects for direct detection*, *Nucl. Phys. B* **706** (2005) 411 [hep-ph/0407218] [INSPIRE].

[58] H. Baer, A. Mustafayev, E.-K. Park, S. Profumo and X. Tata, *Mixed Higgsino dark matter from a reduced* SU(3) *gaugino mass: Consequences for dark matter and collider searches*, *JHEP* **04** (2006) 041 [hep-ph/0603197] [INSPIRE].

[59] I. Gogoladze, F. Nasir, Q. Shafi and C.S. Un, *Nonuniversal Gaugino Masses and Muon g-2*, *Phys. Rev. D* **90** (2014) 035008 [arXiv:1403.2337] [INSPIRE].

[60] S.P. Martin, *Non-universal gaugino masses from non-singlet F-terms in non-minimal unified models*, *Phys. Rev. D* **79** (2009) 095019 [arXiv:0903.3568] [INSPIRE].

[61] D. Feldman, Z. Liu and P. Nath, *Gluino NLSP, Dark Matter via Gluino Coannihilation, and LHC Signatures*, *Phys. Rev. D* **80** (2009) 015007 [arXiv:0905.1148] [INSPIRE].

[62] A.S. Belyaev, S.F. King and P.B. Schaefers, *Muon g-2 and dark matter suggest nonuniversal gaugino masses:* SU(5) × A_4 *case study at the LHC*, *Phys. Rev. D* **97** (2018) 115002 [arXiv:1801.00514] [INSPIRE].

[63] F. Staub, *xBIT: an easy to use scanning tool with machine learning abilities*, arXiv:1906.03277 [INSPIRE].

[64] W. Porod, *SPheno, a program for calculating supersymmetric spectra, SUSY particle decays and SUSY particle production at* e^+e^- *colliders*, *Comput. Phys. Commun.* **153** (2003) 275 [hep-ph/0301101] [INSPIRE].

[65] W. Porod and F. Staub, *SPheno 3.1: Extensions including flavour, CP-phases and models beyond the MSSM*, *Comput. Phys. Commun.* **183** (2012) 2458 [arXiv:1104.1573] [INSPIRE].

[66] F. Staub and W. Porod, *Improved predictions for intermediate and heavy Supersymmetry in the MSSM and beyond*, *Eur. Phys. J. C* **77** (2017) 338 [arXiv:1703.03267] [INSPIRE].

[67] J. Bernon and B. Dumont, *Lilith: a tool for constraining new physics from Higgs measurements*, *Eur. Phys. J. C* **75** (2015) 440 [arXiv:1502.04138] [INSPIRE].

[68] S. Kraml, T.Q. Loc, D.T. Nhung and L.D. Ninh, *Constraining new physics from Higgs measurements with Lilith: update to LHC Run 2 results*, *SciPost Phys.* **7** (2019) 052 [arXiv:1908.03952] [INSPIRE].

[69] P. Bechtle, S. Heinemeyer, O. Stål, T. Stefaniak and G. Weiglein, *HiggsSignals: Confronting arbitrary Higgs sectors with measurements at the Tevatron and the LHC*, *Eur. Phys. J. C* **74** (2014) 2711 [arXiv:1305.1933] [ɪɴSPIRE].

[70] P. Bechtle et al., *HiggsBounds-5: Testing Higgs Sectors in the LHC 13 TeV Era*, *Eur. Phys. J. C* **80** (2020) 1211 [arXiv:2006.06007] [ɪɴSPIRE].

[71] C.K. Khosa, S. Kraml, A. Lessa, P. Neuhuber and W. Waltenberger, *SModelS database update v1.2.3*, arXiv:2005.00555 [ɪɴSPIRE].

[72] S. Kraml et al., *SModelS: a tool for interpreting simplified-model results from the LHC and its application to supersymmetry*, *Eur. Phys. J. C* **74** (2014) 2868 [arXiv:1312.4175] [ɪɴSPIRE].

[73] S. Kraml et al., *SModelS v1.0: a short user guide*, arXiv:1412.1745 [ɪɴSPIRE].

[74] D. Barducci et al., *Collider limits on new physics within MicrOMEGAs_4.3*, *Comput. Phys. Commun.* **222** (2018) 327 [arXiv:1606.03834] [ɪɴSPIRE].

[75] D. Feldman, Z. Liu, P. Nath and G. Peim, *Multicomponent Dark Matter in Supersymmetric Hidden Sector Extensions*, *Phys. Rev. D* **81** (2010) 095017 [arXiv:1004.0649] [ɪɴSPIRE].

[76] D. Feldman, P. Fileviez Perez and P. Nath, *R-parity Conservation via the Stueckelberg Mechanism: LHC and Dark Matter Signals*, *JHEP* **01** (2012) 038 [arXiv:1109.2901] [ɪɴSPIRE].

[77] A. Aboubrahim and P. Nath, *LHC phenomenology with hidden sector dark matter: a long-lived stau and heavy Higgs in an observable range*, in *Meeting of the Division of Particles and Fields of the American Physical Society*, Boston U.S.A. (2019) [arXiv:1909.08684] [ɪɴSPIRE].

[78] A. Aboubrahim, W.-Z. Feng, P. Nath and Z.-Y. Wang, *A multi-temperature universe can allow a sub-MeV dark photon dark matter*, arXiv:2103.15769 [ɪɴSPIRE].

[79] H. Baer, V. Barger, D. Sengupta and X. Tata, *Is natural higgsino-only dark matter excluded?*, *Eur. Phys. J. C* **78** (2018) 838 [arXiv:1803.11210] [ɪɴSPIRE].

[80] J. Halverson, C. Long and P. Nath, *Ultralight axion in supersymmetry and strings and cosmology at small scales*, *Phys. Rev. D* **96** (2017) 056025 [arXiv:1703.07779] [ɪɴSPIRE].

[81] ATLAS collaboration, *Search for electroweak production of charginos and sleptons decaying into final states with two leptons and missing transverse momentum in $\sqrt{s} = 13\,TeV\,pp$ collisions using the ATLAS detector*, *Eur. Phys. J. C* **80** (2020) 123 [arXiv:1908.08215] [ɪɴSPIRE].

[82] ATLAS collaboration, *Searches for electroweak production of supersymmetric particles with compressed mass spectra in $\sqrt{s} = 13\,TeV\,pp$ collisions with the ATLAS detector*, *Phys. Rev. D* **101** (2020) 052005 [arXiv:1911.12606] [ɪɴSPIRE].

[83] CMS collaboration, *Search for supersymmetric partners of electrons and muons in proton-proton collisions at $\sqrt{s} = 13\,TeV$*, *Phys. Lett. B* **790** (2019) 140 [arXiv:1806.05264] [ɪɴSPIRE].

[84] CMS collaboration, *Search for supersymmetry in final states with two oppositely charged same-flavor leptons and missing transverse momentum in proton-proton collisions at $\sqrt{s} = 13\,TeV$*, *JHEP* **04** (2021) 123 [arXiv:2012.08600] [ɪɴSPIRE].

[85] A. Aboubrahim and P. Nath, *Supersymmetry at a 28 TeV hadron collider: HE-LHC*, *Phys. Rev. D* **98** (2018) 015009 [arXiv:1804.08642] [INSPIRE].

[86] A. Aboubrahim and P. Nath, *Naturalness, the hyperbolic branch, and prospects for the observation of charged Higgs bosons at high luminosity LHC and 27 TeV LHC*, *Phys. Rev. D* **98** (2018) 095024 [arXiv:1810.12868] [INSPIRE].

[87] M. Cepeda et al., *Report from Working Group 2*: Higgs Physics at the HL-LHC and HE-LHC, *CERN Yellow Rep. Monogr.* **7** (2019) 221 [arXiv:1902.00134] [INSPIRE].

[88] X. Cid Vidal et al., *Report from Working Group 3*: Beyond the Standard Model physics at the HL-LHC and HE-LHC, *CERN Yellow Rep. Monogr.* **7** (2019) 585 [arXiv:1812.07831] [INSPIRE].

[89] A. Buckley, *PySLHA: a Pythonic interface to SUSY Les Houches Accord data*, *Eur. Phys. J. C* **75** (2015) 467 [arXiv:1305.4194] [INSPIRE].

[90] J. Debove, B. Fuks and M. Klasen, *Joint Resummation for Gaugino Pair Production at Hadron Colliders*, *Nucl. Phys. B* **849** (2011) 64 [arXiv:1102.4422] [INSPIRE].

[91] B. Fuks, M. Klasen, D.R. Lamprea and M. Rothering, *Precision predictions for electroweak superpartner production at hadron colliders with Resummino*, *Eur. Phys. J. C* **73** (2013) 2480 [arXiv:1304.0790] [INSPIRE].

[92] A. Buckley et al., *LHAPDF6: parton density access in the LHC precision era*, *Eur. Phys. J. C* **75** (2015) 132 [arXiv:1412.7420] [INSPIRE].

[93] T. Sjöstrand et al., *An introduction to PYTHIA 8.2*, *Comput. Phys. Commun.* **191** (2015) 159 [arXiv:1410.3012] [INSPIRE].

[94] M. Cacciari, G.P. Salam and G. Soyez, *FastJet User Manual*, *Eur. Phys. J. C* **72** (2012) 1896 [arXiv:1111.6097] [INSPIRE].

[95] M. Cacciari, G.P. Salam and G. Soyez, *The anti-k_t jet clustering algorithm*, *JHEP* **04** (2008) 063 [arXiv:0802.1189] [INSPIRE].

[96] DELPHES 3 collaboration, *DELPHES 3, A modular framework for fast simulation of a generic collider experiment*, *JHEP* **02** (2014) 057 [arXiv:1307.6346] [INSPIRE].

[97] C.G. Lester and D.J. Summers, *Measuring masses of semiinvisibly decaying particles pair produced at hadron colliders*, *Phys. Lett. B* **463** (1999) 99 [hep-ph/9906349] [INSPIRE].

[98] A. Barr, C. Lester and P. Stephens, *m(T2): The Truth behind the glamour*, *J. Phys. G* **29** (2003) 2343 [hep-ph/0304226] [INSPIRE].

[99] C.G. Lester and B. Nachman, *Bisection-based asymmetric M_{T2} computation: a higher precision calculator than existing symmetric methods*, *JHEP* **03** (2015) 100 [arXiv:1411.4312] [INSPIRE].

[100] P. Speckmayer, A. Hocker, J. Stelzer and H. Voss, *The toolkit for multivariate data analysis, TMVA 4*, *J. Phys. Conf. Ser.* **219** (2010) 032057 [INSPIRE].

[101] I. Antcheva et al., *ROOT: A C++ framework for petabyte data storage, statistical analysis and visualization*, *Comput. Phys. Commun.* **182** (2011) 1384 [INSPIRE].

[102] S. Iwamoto, T.T. Yanagida and N. Yokozaki, *Wino-Higgsino dark matter in the MSSM from the $g-2$ anomaly*, arXiv:2104.03223 [INSPIRE].

[103] Y. Gu, N. Liu, L. Su and D. Wang, *Heavy Bino and Slepton for Muon g-2 Anomaly*, arXiv:2104.03239 [INSPIRE].

[104] M. Van Beekveld, W. Beenakker, M. Schutten and J. De Wit, *Dark matter, fine-tuning and $(g-2)_\mu$ in the pMSSM*, arXiv:2104.03245 [INSPIRE].

[105] W. Yin, *Muon $g-2$ Anomaly in Anomaly Mediation*, arXiv:2104.03259 [INSPIRE].

[106] F. Wang, L. Wu, Y. Xiao, J.M. Yang and Y. Zhang, *GUT-scale constrained SUSY in light of E989 muon g-2 measurement*, arXiv:2104.03262 [INSPIRE].

[107] J. Cao, J. Lian, Y. Pan, D. Zhang and P. Zhu, *Improved $(g-2)_\mu$ Measurement and Singlino dark matter in the general NMSSM*, arXiv:2104.03284 [INSPIRE].

[108] M. Chakraborti, S. Heinemeyer and I. Saha, *The new "MUON G-2" Result and Supersymmetry*, arXiv:2104.03287 [INSPIRE].

[109] P. Cox, C. Han and T.T. Yanagida, *Muon $g-2$ and Co-annihilating Dark Matter in the MSSM*, arXiv:2104.03290 [INSPIRE].

[110] C. Han, *Muon g-2 and CP-violation in MSSM*, arXiv:2104.03292 [INSPIRE].

[111] S. Baum, M. Carena, N.R. Shah and C.E.M. Wagner, *The Tiny (g-2) Muon Wobble from Small-µ Supersymmetry*, arXiv:2104.03302 [INSPIRE].

[112] W. Ahmed, I. Khan, J. Li, T. Li, S. Raza and W. Zhang, *The Natural Explanation of the Muon Anomalous Magnetic Moment via the Electroweak Supersymmetry from the GmSUGRA in the MSSM*, arXiv:2104.03491 [INSPIRE].

[113] H. Baer, V. Barger and H. Serce, *Anomalous muon magnetic moment, supersymmetry, naturalness, LHC search limits and the landscape*, arXiv:2104.07597 [INSPIRE].

[114] M. Endo, K. Hamaguchi, S. Iwamoto and T. Kitahara, *Supersymmetric Interpretation of the Muon $g-2$ Anomaly*, arXiv:2104.03217 [INSPIRE].

[115] M. Ibe, S. Kobayashi, Y. Nakayama and S. Shirai, *Muon $g-2$ in Gauge Mediation without SUSY CP Problem*, arXiv:2104.03289 [INSPIRE].

[116] M. Chakraborti, L. Roszkowski and S. Trojanowski, *GUT-constrained supersymmetry and dark matter in light of the new $(g-2)_\mu$ determination*, arXiv:2104.04458 [INSPIRE].

[117] W. Altmannshofer, S. Aditya Gadam, S. Gori and N. Hamer, *Explaining $(g-2)_\mu$ with Multi-TeV Sleptons*, arXiv:2104.08293 [INSPIRE].

[118] P. Athron, C. Balazs, D.H.J. Jacob, W. Kotlarski, D. Stockinger and H. Stockinger-Kim, *New physics explanations of a_μ in light of the FNAL muon $g-2$ measurement*, arXiv:2104.03691 [INSPIRE].